Available online at www.sciencedirect.com
ScienceDirect
Ceramics International 34 (2008) 1145–1152
CERAMICS INTERNATIONAL
www.elsevier.com/locate/ceramint

Low temperature production of glass ceramics in the anorthite–diopside system via sintering and crystallization of glass powder compacts

V.M.F. Marques [a], D.U. Tulyaganov [a,b], S. Agathopoulos [a], J.M.F. Ferreira [a,*]

[a] Department of Ceramics and Glass Engineering, University of Aveiro, CICECO, 3810-193 Aveiro, Portugal
[b] Scientific Research Institute of Space Engineering, 700128 Tashkent, Uzbekistan

Received 16 November 2006; received in revised form 18 January 2007; accepted 6 February 2007
Available online 6 March 2007

Abstract

The production of glass ceramics (GCs) with theoretical anorthite–diopside (An–Di) weight ratios of 60/40, 50/50 and 45/55 via sintering and crystallization of glass powder compacts was investigated at different temperatures between 800 and 950 °C. The investigated compositions are located in the cross-section of the ternary fluorapatite–An–Di system close to An–Di binary joint, with constant fluorapatite content of 4.8 wt.%. Two different groups of glass powders, with mean particle size of 2 and 10 μm, were used. The experimental results showed that sintering is almost complete at 800 °C, preceding crystallization, which takes place via surface crystallization mechanism. The properties values of the produced GCs, which are the best for the composition close to An–Di eutectic line, are discussed with respect to the evolution of crystalline phases and the microstructure over increasing firing temperature. Under the technology perspective, the investigated processing route is significantly superior in comparison to the attempts reported in earlier studies.

Keywords: A: Sintering; D: Glass; D: Glass ceramics; Anorthite–diopside

1. Introduction

Anorthite (An, $CaAl_2Si_2O_8$) and diopside (Di, $CaMgSi_2O_6$) are widely spread in nature and belong to the plagioclase and pyroxene group of rock forming minerals, respectively. Plagioclases represent a sequence of solid solutions between An and albite ($NaAlSi_3O_8$) resulting in a big group of triclinic minerals. Plagioclases are framework silicates where each silica tetrahedra share all corners with its neighbouring thetrahedra. A portion of tetrahedra contains Al^{3+} instead of Si^{4+} and the charge is balanced by incorporation Na^+ or Ca^{2+}. The properties of An are as follows: density of 2.74–2.76 g/cm^3, hardness of 6–7 in Mohs scale and melting point at 1553 °C [1]. Glass ceramics (GCs) and ceramics of An are used in electrical, thermo-mechanical and water resistant applications [2–5]. On the other hand, pyroxenes are actually built on single chains of SiO_4 tetrahedra. In Di, which crystallizes in monoclinic lattice, two silicate chains are joined together via Mg^{2+} occupying symmetrical (or regular) octahedral positions and Ca^{2+} that fills irregular octahedral positions. The properties of Di are: density of 3.27 g/cm^3, hardness of 5–6 in Mohs scale and melting point at 1391 °C [1]. The high mechanical and chemical durability [6–9] of Di-based glasses and GCs justify their wide use in several applications.

The binary An–Di system has been thoroughly documented [10]. Accordingly, the An–Di phase diagram is of a simple eutectic type with no solid solutions. The eutectic point corresponds to 42% An and 58% Di (in wt.%) and melts at 1274 °C. The An–Di system attracts special industrial interest because of the possibility of introducing inexpensive and abundant, in nature, raw materials in glass batches, the relatively simple conditions of melting and ceramization, and the possibility to obtain GCs with wide range of An/Di ratios [1,11,12].

Leonelli et al. [12] have studied the nucleation and crystallization mechanisms of three An–Di glasses with theoretical An/Di ratio (in wt.%) of 75/25, 50/50 and 25/75. Glasses, produced by quenching either in frit or bulk form, were completely crystallized via simple surface nucleation. Complete densification was attained with no addition of nucleating

* Corresponding author. Tel.: +351 234 370242; fax: +351 234 425300.
E-mail address: jmf@cv.ua.pt (J.M.F. Ferreira).

0272-8842/$34.00
doi:10.1016/j.ceramint.2007.02.008

agents. The glasses with An/Di ratio of 75/25 were predominantly crystallized to An, but that glass was inherently prone to intensive devitrification, even via quenching of glass melt. The problem to get true glass makes difficult the control of sintering and crystallization. Corradi et al. [13], who applied molecular dynamic simulations to determine the distribution of Si atoms in these glasses, found a progressive shift from Q^2 to Q^4 species going from Di to An edge. Rietveld-RIR analysis has been also applied by Barbieri et al. [14] in a detailed structural and devitrification study of several An–Di glass compositions. In that study, samples of glasses in bulk form were heat treated at different temperatures (between 900 and 1200 °C) and times. Those conditions were suggested from the results of differential thermal analysis (DTA) with fine powders (mean particle sizes <25 μm), whereby the crystallization peaks were registered in the range of 900–930 °C. The experimental results of crystallization of bulk glass samples showed that GCs with significant amount of crystalline phase were obtained after heat treatment at 1000 °C for 4 h, or at 1100 °C for 1 h. There was obviously a noticeable difference between the results of DTA and the crystallization of the bulk glass samples.

The addition of fluorapatite (FA, $Ca_5(PO_4)_3F$) in An–Di system has been also thoroughly documented in a study on phase equilibria in the ternary FA–An–Di system [15], which has demonstrated that FA beneficially widens the glass-forming region along the An–Di boundary. According to that important finding and in the light of the poor systematic experimental documentation on sintering and crystallization of An–Di glass powder compacts, the authors have studied [16] the production and characterization of three An-based GCs, with compositions marked as A–C in Fig. 1, which had theoretical An/Di ratio (in wt.%) of 90/10, 80/20 and 70/30, respectively. The ultimate reasoning for developing those compositions was the potential use of the GCs as LTCC (low temperature co-fired ceramics) substrates. From the technology point of view, that study has shown that transparent, bubble-free and colourless glass frits could be obtained via melting at 1500–1580 °C for 1.5 h and subsequent quenching.

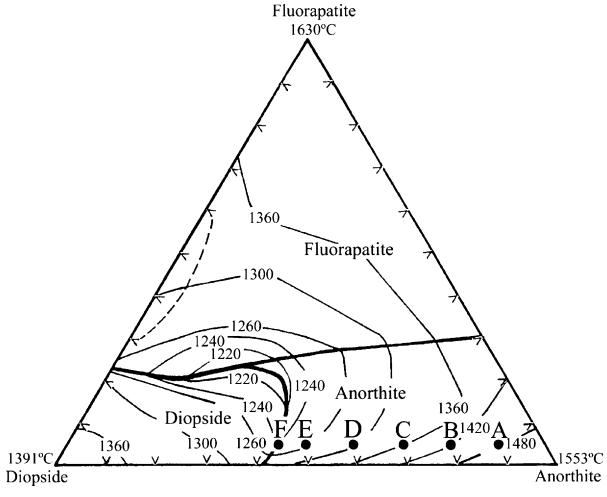

Fig. 1. The investigated compositions D, E and F in the fragment of fluorapatite-diopside–anorthite ternary diagram (in wt.%) [15]. The compositions A, B, and C studied in Ref. [16] are also shown. (B_2O_3-doping has not been considered).

The dependence of DTA plots on powder particle size indicated that these glasses devitrify via surface crystallization mechanism. Hence, sintering of glass powder compacts proved to be a good processing method for producing GCs of those compositions. The sintering behaviour, the crystallization and the properties of glass powder compacts with mean particle sizes of 2 and 10 μm were investigated at different temperatures between 800 and 950 °C. In the specimens of the finer particles (2 μm), complete densification was achieved at a noticeably low temperature (825 °C) and the highest mechanical strength was obtained at 850 °C, but density significantly decreased at higher temperatures. Bending strength generally increases in the order A < B < C (the highest values were 112–115, 122–130 and 131–140 MPa, respectively). The coefficients of thermal expansion (CTE) of the sintered GCs were $4.62–5.10 \times 10^{-6}\ K^{-1}$ (100–500 °C) and generally increased from composition A to C.

The present study aims to expand the documentation in the FA–An–Di ternary system towards Di-richer compositions up to the An–Di boarder, maintaining the same FA-content at 4.8 wt.% (like in A–C [16]). The three new compositions investigated in the present paper are denoted with the letters D–F and pointed in the diagram of Fig. 1, corresponding to An/Di weight ratios of 60/40, 50/50, and 45/55, respectively. The properties of the new GCs are compared to GCs A–C. According to Fig. 1, the liquidus temperatures of the previously investigated compositions A–C [16] should be 1480, 1420, and 1360 °C, respectively, while for the new compositions D–F the liquidus temperatures decrease to 1300, 1260, and 1240 °C, respectively.

2. Materials and experimental procedure

Powders of technical grade of SiO_2 (purity > 99.5%) and $CaCO_3$ (>99.5%), and of reactive grade of MgO, Al_2O_3, CaF_2, and $NH_4H_2PO_4$ were used. To enhance melt fluidity as well as sinterability of GCs, the compositions D and E were doped with 2 and 1 wt.% B_2O_3, respectively. The batch compositions of the glasses are shown in Table 1. Homogeneous mixtures of batches (100 g), obtained by thorough ball milling, were preheated at 1000 °C for 1 h for decarbonization. Melting was successfully carried out in alumina crucibles in air at 1450–1500 °C for 1 h.

Glass frits were obtained by quenching of melts into cold water. The frits were dried and then milled in a high-speed porcelain mill in absolute ethanol. To investigate the influence of particle size of glass powders on the properties of GCs, the

Table 1
Chemical compositions of glass batches (wt.%)

Composition	SiO_2	Al_2O_3	CaO	MgO	P_2O_5	CaF_2	B_2O_3
D	44.91	20.52	23.32	6.95	1.98	0.36	1.96
E	46.50	17.28	24.09	8.77	2.00	0.37	0.99
F	47.57	15.69	24.60	9.75	2.02	0.37	–

milling conditions (i.e. time, weight ratio of glass frit/porcelain balls and spinning rate) were adjusted in a way to produce a group of fine powders (mean particle size ca. 2 μm) and a group of coarse powders (ca. 10 μm). Rectangular bars (4 mm × 5 mm × 50 mm) of glass powder compacts were produced by uniaxial pressing (80 MPa) using fine and coarse powders. The bars were heat-treated in air in an electric laboratory furnace at different temperatures of 800, 825, 850, 900, and 950 °C. The heating and cooling rates were 5 °C/min with 1 h soaking at the highest sintering temperatures.

The following techniques were used. The particle size distribution of the powders was determined by light scattering technique (Coulter LS 230, UK, Fraunhofer optical model). Differential thermal analysis (DTA) was carried out in air (Labsys Setaram TG-DTA/DSC, France; heating rate 5 °C/min). The thermal expansion measurements were done with a dilatometer (Bahr Thermo Analyse DIL 801 L, Germany; heating rate 5 °C/min; samples cross-section 4 mm × 5 mm). The crystallized phases were determined by X-ray diffraction analysis (XRD, Rigaku Geigerflex D/Mac, C Series, Cu Kα radiation, Japan). Microstructure observations were carried out on fracture surfaces by scanning electron microscopy (SEM, Hitachi S-4100, Japan, 25 kV acceleration voltage) at etched GCs by immersing the samples in 2 vol.% HF solution for 10 s. The apparent density was measured by the Archimedes method (i.e. immersion in ethylenoglycol). The linear shrinkage during sintering was calculated from the dimensions of the green and of the sintered samples. The evaluation of mechanical properties comprised measurements of Vickers microhardness (Shimadzu microhardness tester type M, Japan, load of 1.96 N; each value is the mean value of 50 indentations made on five different samples, i.e. 10 measurements at each sample), and three-point bending strength of rectified parallelepiped bars (3 mm × 4 mm × 50 mm) of sintered GCs (Shimadzu Autograph AG 25 TA, 0.5 mm/min displacement; each value is the mean value of measurements obtained from 12 bars). Water absorption was evaluated according to the ISO-standard 10545-3, 1995 (i.e. weight gain of samples after immersion into boiling water for 2 h). The chemical resistance was evaluated by immersion of prismatic samples (22.5 mm × 4.5 mm × 4.0 mm) into solutions of 5% NaOH, and 5% HCl at 95 °C for 24 h. Vickers microhardness and chemical resistance of GCs A, B and C were evaluated from the samples obtained in the study [16].

3. Results and discussion

The investigated glasses were successfully melted at the chosen melting conditions. Their casting ability was also very good. After quenching in cold water, the resultant frits were bubble-free, transparent, and colourless. X-ray diffraction analysis of frits confirmed their absolute vitreous state and the absence of devitrification. The plots of the particle size distributions of the fine (mean particle size ca. 2 μm) and the coarse (ca. 10 μm) powders are presented in Fig. 2.

The DTA plots of the fine and the coarse glass powders of the three glasses D, E and F are presented in Fig. 3. The

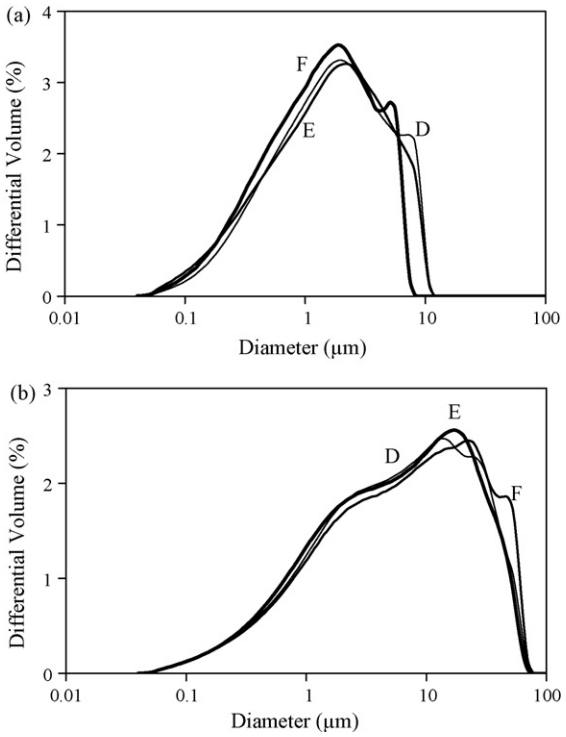

Fig. 2. Particle size distributions of the glass powders with mean particle size of (a) ca. 2 μm, and (b) ca. 10 μm.

characteristic points (T_g and crystallization peaks, T_p) from these plots are summarized in Table 2 together with the values for the glasses A, B and C [16]. These values suggest the following general features along that series of compositions (i.e. from A to F):

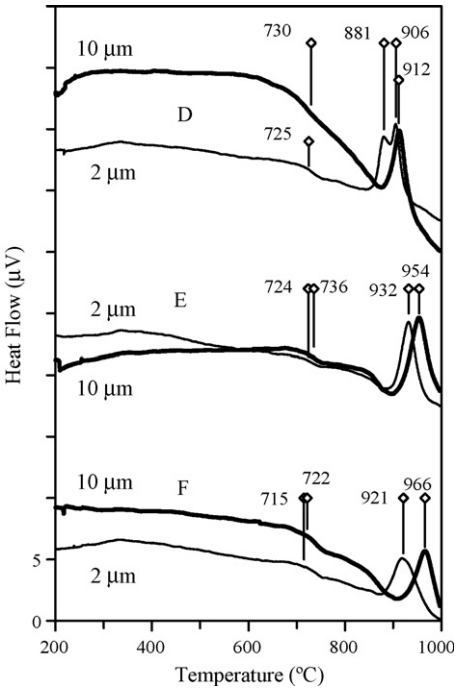

Fig. 3. Differential thermal analysis (DTA) plots of the investigated glasses.

Table 2
Characteristic temperatures determined from DTA

Glass	T_g		T_{p1}		T_{p2}	
	2 μm	10 μm	2 μm	10 μm	2 μm	10 μm
A[a]	755	770	890	907		
B[a]	745	761	877	899		
C[a]	738	753	871	911	892	930
D	725	730	881	912	906	
E	724	736	932	954		
F	715	722	921	966		

[a] The T_g and T_p values for compositions A, B and C are from Ref. [16].

(a) The glass transition (T_g), which has as a shallow endothermic effect before the crystallisation peaks, shifts to higher temperatures with increasing An portion or CaO/MgO ratio. This is attributed to the role of Al^{3+} in the structure of glasses. Ca^{2+} cations favour the substitution of silicon for aluminium, the appearance of a portion of tetrahedra containing Al^{3+} instead of Si^{4+} and the polymerization of the glass network. In the contrast, Mg^{2+} cations stabilise aluminium in the octahedral coordination and Al^{3+} acts as a modificator in the glass structure [1].
(b) The increase of mean particle size from 2 to 10 μm causes a shift of crystallization peaks to higher temperatures, suggesting surface crystallization as the dominant mechanism in the investigated compositions [5,12,17].

Sintering of glass powder compacts generally starts at temperatures slightly higher than T_g due to viscous flow, which instigates coalescence of the powder and removes the pores from the bulk of materials [5,6]. Accordingly, in the investigated glasses, densification should start at about 720–730 °C (Fig. 3), likely by viscous coalescence, and progresses at high temperatures. It is worthy noting that the heating rate in all DTAs and in the sintering experiments was of 5 °C/min. Fully dense glass powder compacts were obtained after firing at 800 °C suggesting that sintering is almost complete at that temperature. Further XRD analysis of those samples confirmed their amorphous nature, which, in conjunction with the properties (discussed below) and the DTA plots (Fig. 3) suggests that sintering precedes crystallization.

The influence of temperature of heat treatment (from 800 to 950 °C) on the quality of the produced materials, as reflected on density, water absorption, and shrinkage, is summarized in Figs. 4 and 5. The highest values of density and shrinkage along with zero water absorption were obtained at 825 °C for the samples made of fine powders and at 850 °C for the samples made of coarse powders. These results agree fairly well with the earlier results with the compositions A, B and C [16].

However, the differences among the compositions D, E, and F are not as much striking as already observed among the compositions A, B and C. This means that the investigated compositions D, E and F, which are richer in Di, exhibit better stability of properties values over a wide temperature range than the compositions A, B and C. Similarly to compositions A, B and C, coarse powders (10 μm) enhanced the thermal stability of D, E and F compositions since the samples made of

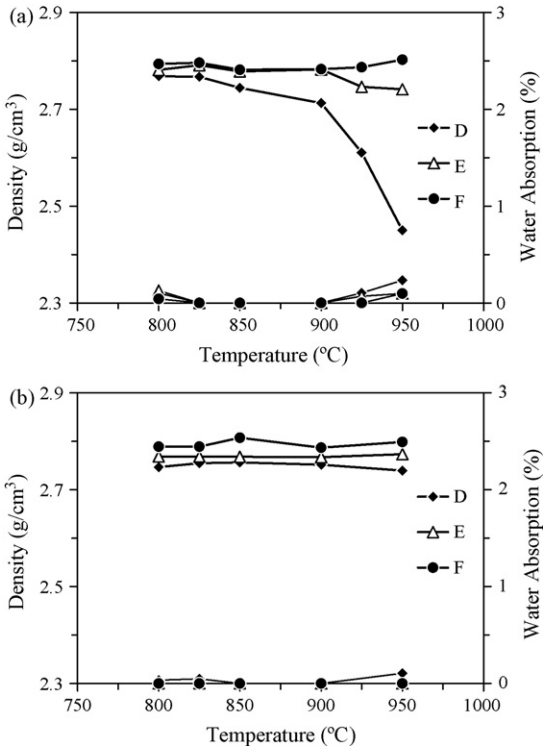

Fig. 4. Influence of temperature of heat treatment on density and water absorption of samples made of powders with mean particle sizes of (a) 2 μm and (b) 10 μm. (The standard deviation of the presenting points is less than 5%.)

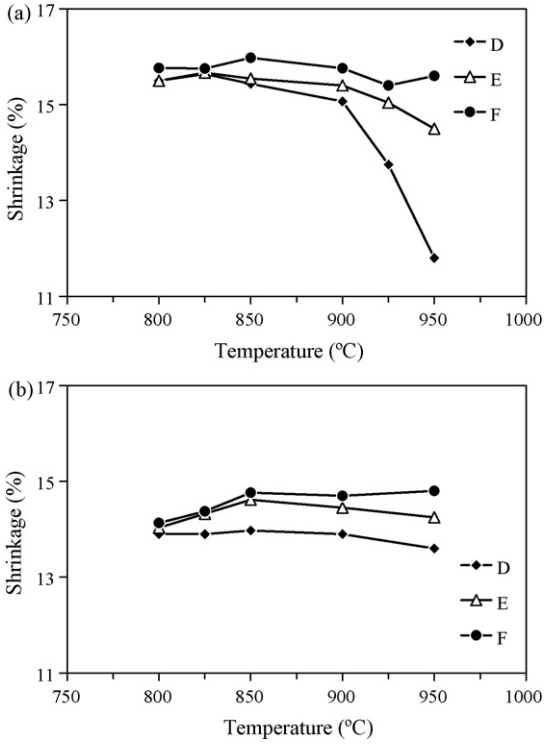

Fig. 5. Influence of temperature of heat treatment on shrinkage of samples made of powders with mean particle sizes of (a) 2 μm and (b) 10 μm. (The standard deviation of the presenting points is less than 5%.)

the fine powders (2 μm) featured significant decay of density and shrinkage after heat treatment at temperatures higher than 850 °C. It is also worth noting that the properties values of the samples of composition F are generally the best, being practically independent on particle size and temperature (825–900 °C).

With regards to mechanical properties, the particle size seems to have little influence on three-point bending strength of the samples heat treated between 800 and 900 °C (Fig. 6). Samples made with the coarse particles (10 μm) were, however, considerably stronger that those with fine powers (2 μm) after firing at temperatures higher than 900 °C. This finding might be correlated to the thermographs of Fig. 3, where the coarse particles (10 μm) have caused a shift of crystallization peaks to higher temperatures. Along the entire series of compositions of Fig. 1 (i.e. from A to F), it is concluded that increasing portion of Di results in stronger GCs. Under the technological perspective, the three-point bending strength values are summarized as 112–115 MPa for A, 122–130 MPa for B, 131–140 for C [16], 148–152 MPa for D, 158–166 MPa for E, and 165–200 MPa for F. Similar tendencies are generally observed in the values of Vickers microhardness of GCs fired at 900 °C and summarized in Table 3 (there is merely a slight discrepancy for composition E).

The CTE values, calculated from the slopes of the linear parts of the dilatation curves (not shown) between 100 and 500 °C, of GCs from 10 μm size powders fired at 900 °C are summarized in Table 4 together with the CTEs of the GCs A, B and C [16]. There is evidently a wide range of CTE values,

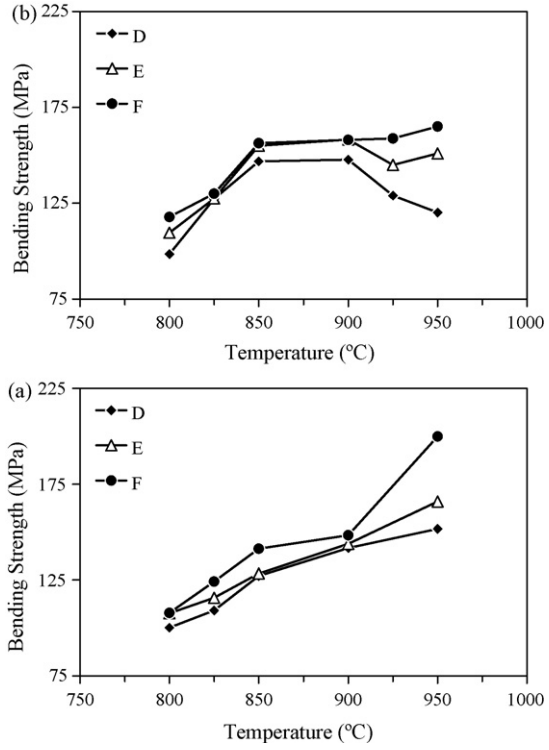

Fig. 6. Influence of temperature of heat treatment on three-point bending strength of samples made of powders with mean particle sizes of (a) 2 μm and (b) 10 μm. (The standard deviation of the presenting points is less than 5%.)

Table 3
Vickers microhardness (in HV) of the glass ceramics (GC) A–C [16], D–F, made with powders of 2 and 10 μm, and sintered at 900 °C

GC	Vickers microhardness (HV)	
	2 μm	10 μm
A	315.80 ± 4.42	353.38 ± 26.80
B	322.58 ± 5.52	451.34 ± 15.62
C	412.64 ± 21.31	573.38 ± 12.15
D	497.12 ± 9.60	591.94 ± 10.39
E	464.65 ± 3.52	507.12 ± 5.13
F	558.22 ± 16.63	619.16 ± 18.59

making these GCs attractive for producing composite materials where the good matching of CTEs between the dissimilar materials is of great importance for the long term functionality and structural integrity of the resultant composites. The general trend is that CTE increases from A to F (i.e. by increasing Di portion).

The chemical resistance (expressed in terms of dissolved mass per exposed unit area) of the GCs of the entire series (i.e. from A to F) fired at 900 °C in alkaline and acidic environment is summarized in Table 5. Evidently, the produced GCs are pronouncedly resistant in alkaline environment but highly vulnerable to acidic chemical attack. The fine powers (2 μm) resulted in GCs with lower chemical resistance likely due to the higher values of porosity and water absorption, and to the lower degree of crystallinity of the samples [16]. On the other hand, increasing An seems to enhance the chemical vulnerability particularly to acid attack, while increasing Di improves the chemical resistance of GCs.

Table 4
Coefficients of thermal expansion (CTE) of the glass ceramics (GC) A–F, made with powders of 10 μm and sintered at 900 °C, calculated from the slope of the linear parts of the dilatometry curves between 100 and 500 °C

GC	CTE (10^{-6} K^{-1})
A[a]	4.62
B[a]	5.05
C[a]	5.10
D	6.45
E	6.53
F	6.34

[a] The T_g and T_p values for compositions A, B and C are from Ref. [16].

Table 5
Chemical durability (in μg/cm^2) of the glass ceramics (GC) A–F, made with powders of 2 and 10 μm, and sintered at 900 °C, in 5% NaOH and 5% HCl solutions at 95 °C for 24 h

GC	NaOH		HCl	
	2 μm	10 μm	2 μm	10 μm
A	1.126	0.518	ds	186
B	0.901	0.518	ds	182
C	0.821	0.522	ds	81.9
D	0.701	0.602	97.4	66.1
E	0.678	0.516	94.2	31.9
F	0.535	0.515	25.5	10.3

ds: The samples were entirely dissolved.

The above reported properties should be related to the crystalline phases formed in the GCs. The diffractograms of Fig. 7 present the evolution of these phases in the GCs D, E and F made of coarse powders (10 μm) at 850, 900, and 950 °C. The intensities of the X-ray peaks of the GCs made of the fine powers (2 μm) were much weaker (not shown). From the analysis of the diffractograms of Fig. 7, An and Di are predominantly identified. However, there are also other interesting features, summarized as follows.

In the diffractogram of the well-crystallized GC D sintered at 850 °C (Fig. 7a), besides the above two phases (An and Di), akermanite (Ak, $Ca_2MgSi_2O_7$) was also clearly registered. The intensity of Di peaks increased with increasing the temperature, whereas the intensity of An peaks decreased. The peaks of Ak tended to fade out while the most intensive peaks of FA became evident. The diffractograms at 900 and 950 °C are similar in terms of the phases identified and the intensity of their peaks.

The intensity and the sharpness of the An and Di peaks of the GC E sintered at 850 °C (Fig. 7b) are considerably lower than those of the GC D at same temperature. However, the peaks of Ak appear stronger and sharper than in Fig. 7a. The crystallinity of GCs E was considerably improved at 900 °C as suggested mostly by the intensity of Di peaks. FA peaks were also registered, whereas the Ak peaks tended to fade out. The

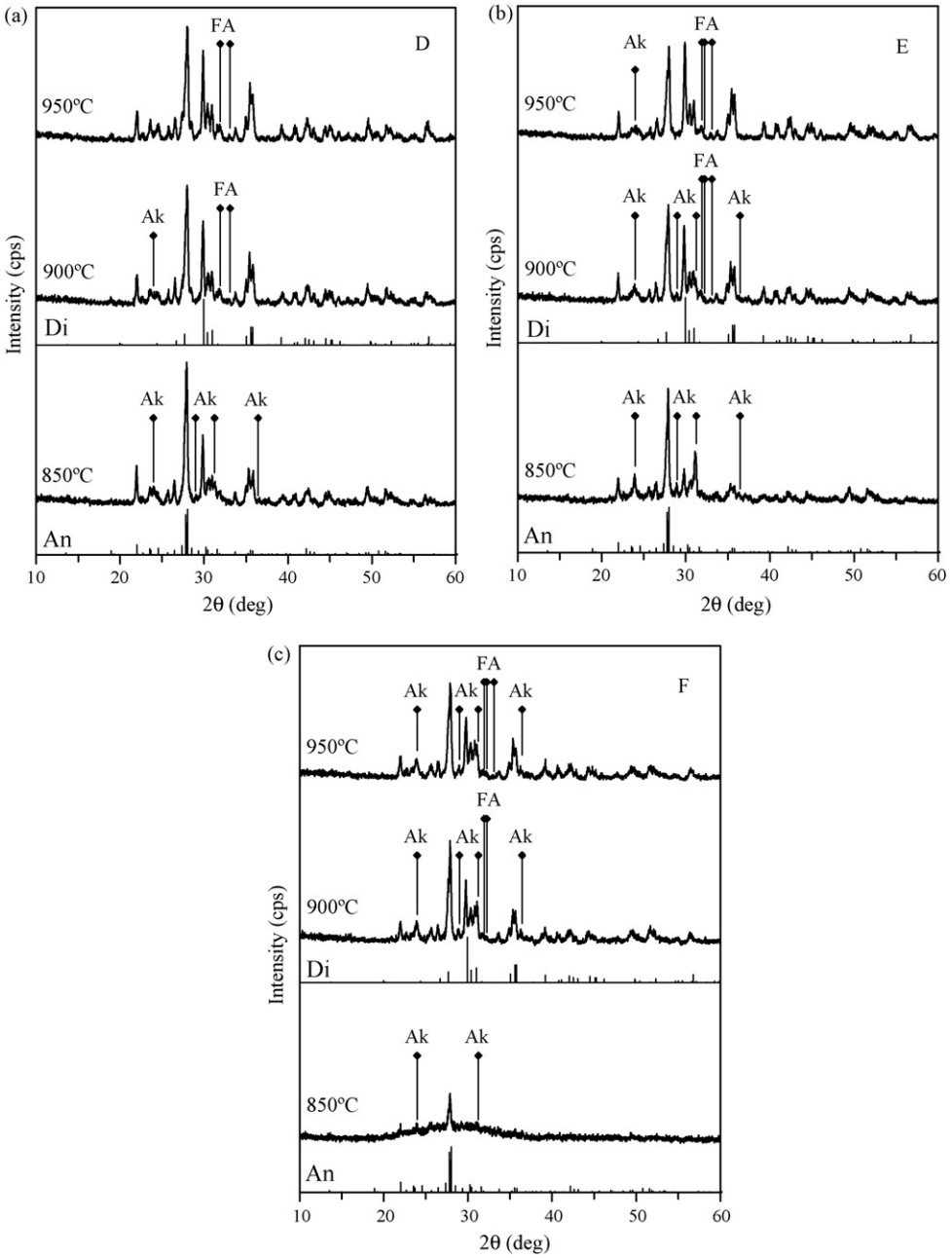

Fig. 7. X-ray diffractograms of glass ceramics (a) D, (b) E, and (c) F fired at different temperatures for 1 h. The patterns of the crystalline phases correspond to anorthite (An, $CaAl_2Si_2O_8$, ICDD card 00-041-1486), diopside (Di, $CaMgSi_2O_6$, 01-075-0945), fluorapatite (FA, $Ca_5(PO_4)_3F$, 01-073-1727), and akermanite (Ak, $Ca_2MgSi_2O_7$, 01-076-0841). The spectra have not been normalized. Full scale 6000 cps.

crystallinity of An and Di phases was significantly enhanced upon heat treating the GCs E at 950 °C, and FA was also identified. In comparison to the GC D heat treated at the same temperature, the peaks of Di are slightly more intense in composition E, likely due to MgO enrichment.

Although the difference between the compositions E and F is seemingly small (Fig. 1), the slight increase of Di components in F caused a considerable decay of crystalline regime of samples heat treated at 850 °C (Fig. 7c). The corresponding diffractogram confirms the presence of a large amount of glassy phase where only small and broad peaks of An and very small (but recognizable after detailed analysis) of Ak were registered, but not Di. Well-crystallized GCs F of An and Di as well as Ak were obtained after sintering at 900 °C. Further increase of temperature to 950 °C caused almost negligible changes to the crystalline regime, which are mostly summarized by a slight decay of Ak peaks intensity and the appearance of small peaks of FA.

Consequently, An forms in all the investigated compositions from the lowest temperatures (i.e. 850 °C). Increase of Di components seemingly causes a decay of crystallinity of GCs, favours Ak formation (which is less stable at higher temperatures), and suppresses formation of Di and FA. Disregarding the FA–An–Di phase diagram [15], the formation of Ak might be explained by considering possible structural rearrangements that take place in the earlier stages of the crystallization process, ensuring partial transformation of octahedrally into tetrahedrally coordinated magnesium and easier formation of silicates of a simpler structure [11,18].

Fig. 8 shows typical microstructures of the GCs D, E, and F made with the coarse powders (10 μm) and sintered at 900 °C. Characteristic lamellar crystals of An and dendrites of Di are observed, being cemented with residual glass in the GCs D (Fig. 8a) and E (Fig. 8b). A considerably different microstructure was developed in the GCs F (Fig. 8c). In particular, two distinguished fields can be observed: a field of fine crystals with lengths less than 1 μm, and a field with relatively coarse crystals of about 3 μm. The former field features coupled eutectic microstructure which should form during eutectic solidification due to the small diffusion distances in the solid state. This feature is in good agreement with the FA–An–Di phase diagram [15], specifically by considering the location of composition F at the eutectic Di–An boundary (Fig. 1). When growth is coordinated, eutectic growth is termed as ''coupled'' [19]. In that case, no phase grows faster than the other. Moreover, the combined growth is faster than the individual growth of each of the constituent phases alone.

In general, there is a fair agreement between the results of DTA (Fig. 3) and XRD (Fig. 7), also supported by the microstructure observations (Fig. 8), since the T_p temperatures (Table 2) correspond fairly well to the temperatures of the maximum X-ray intensities registered at the diffractograms. The high crystallization degree in GCs, as qualitatively suggested by the X-ray diffractograms, should result in the highest mechanical strength values, achieved after heat treatment at 950 °C for 1 h. These findings are different from those reported by Barbieri et al. [14], where GCs in the An–Di system with significant degree of crystallization were obtained after heat treatment of bulk glasses

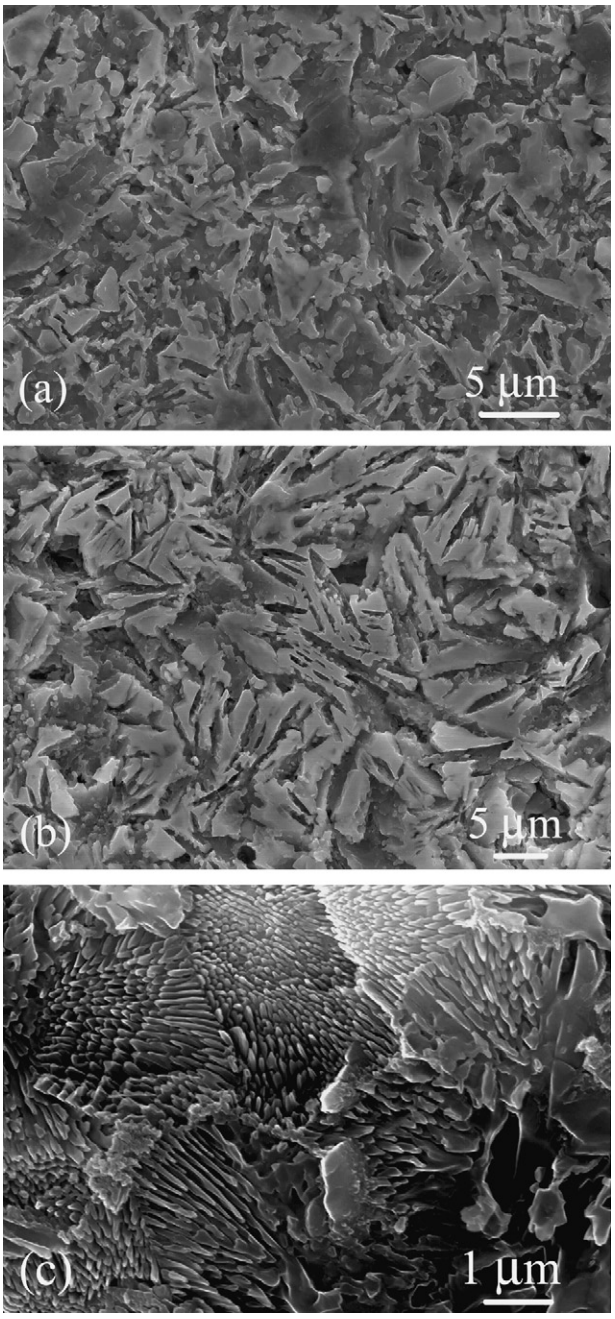

Fig. 8. Typical microstructures of glass ceramics (a) D, (b) E, and (c) F made from coarse particles (10 μm), after sintering at 900 °C for 1 h. (Etching with 2 vol.% HF.)

at 1000 °C for 4 h, or at 1100 °C for 1 h. This sound discrepancy should be attributed to the different preparation routes of GC. As a matter of fact, when surface crystallization predominantes, using fine glass powder compacts shifts crystallization to considerably lower temperatures, while higher temperatures are required for crystallization of bulk glasses [14].

4. Concluding remarks

The results of this study reveal the potential of the investigated series of compositions for industrial applications. The most important points are as follows:

1. An–Di GCs can be produced at relatively low temperatures (850–900 °C) via sintering and crystallization of glass powder compacts.
2. Increasing the An portion in the glass caused a shift of T_g and crystallization peaks to higher temperatures, which may be attributed to the role of Al^{3+} as a network former in the structure of the glasses.
3. Sintering is almost complete at 800 °C and precedes crystallization, which results in GCs of An and Di, together with less FA and Ak (which becomes less stable at higher temperatures).
4. The particle size of the powders influences the quality of the produced GCs. Densification and crystallization occur at lower temperatures when using fine powders than coarser ones. The use of coarse particles favours increase of density and mechanical properties. The highest values of density and shrinkage along with zero water absorption were obtained at 825 and 850 °C for the samples made of fine and coarse powders, respectively.
5. Mechanical strength, CTE and chemical durability increase towards the Di-rich corner. The eutectic An–Di composition F exhibited the best properties, likely due to the fine eutectic microstructure developed during eutectic solidification. A wide spectrum of properties' values, which can fulfil specific applications' requirements.

Acknowledgements

This study was supported by CICECO and the Portuguese Foundation for Science and Technology (FCT).

References

[1] N.M. Pavlushkin, Principals of Glass Ceramics Technology, 2nd ed., Stroiizdat, Moscow, 1979 (in Russian).
[2] E.Y. Medvedovskii, F.Y. Kharitonov, T.D. Shcherbina, Electrical insulating materials based on anorthite, Glass Ceram. (English Translation) 46 (1990) 204–206.
[3] Y. Kobayashi, E. Kato, Low temperature fabrication of anorthite ceramics, J. Am. Ceram. Soc. 77 (1994) 833–834.
[4] I. Yasui, B. Ryu, T. Kawarazaki, Sintering and crystallization behavior of glass powder with composition of anorthite, $CaO{\cdot}Al_2O_3{\cdot}2SiO_2$, in: M.C. Weinberg (Ed.), Nucleation and crystallization in glasses and liquids. Ceram. Trans. 30, The American Ceramic Society, Westerville, OH, 1993, pp. 323–326.
[5] C.L. Lo, J.G. Duh, B.S. Chiou, Low temperature sintering and crystallization behaviour of low loss anorthite-based glass ceramics, J. Mater. Sci. 38 (2003) 693–698.
[6] A. Karamanov, L. Arriza, I. Matekovits, M. Pelino, Properties of sintered glass ceramics in the diopisde–albite system, Ceram. Int. 30 (2004) 2119–2135.
[7] W. Höland, G. Beall, Glass ceramic Technology, The American Ceramic Society, Westerville, OH, 2002.
[8] I.W. Donald, B.L. Metcalfe, R.N.J. Taylor, The immobilization of high level radioactive wastes using ceramics and glasses, J. Mater. Sci. 32 (1997) 5851–5887.
[9] A. Goel, D.U. Tulyaganov, S. Agathopoulos, M.J. Ribeiro, J.M.F. Ferreira, Diopside–Ca–Tschermak clinopyroxene based glass ceramics processed via sintering and crystallization of glass powder compacts, J. Eur. Ceram. Soc. 27 (2007) 2325–2331.
[10] E.F. Osborn, The system wollasonite–diopside–anorthite, Am. J. Sci. 240 (1942) 751–758.
[11] D.U. Tulyaganov, M.J. Ribeiro, J.A. Labrincha, Development of glass ceramics by sintering and crystallisation of fine powders of calcium–magnesium–aluminosilicate glass, Ceram. Int. 28 (2002) 515–520.
[12] C. Leonelli, T. Manfredini, M. Paganelli, P. Pozzi, G.C. Pellacani, Crystallization of some anorthite–diopside glass precursors, J. Mater. Sci. 26 (1991) 5041–5046.
[13] A.B. Corradi, F. Bondioli, V. Cannillo, A.M. Ferrari, I. Lancellotti, M. Montorsi, The anorthite–diopside system: structural and devitrification study. Part I. Structural characterization by molecular dynamic simulations, J. Am. Ceram. Soc. 88 (2005) 714–718.
[14] L. Barbieri, F. Bondioli, I. Lancellotti, C. Leonelli, M. Montorsi, The anorthite–diopside system: structural and devitrification study. Part II. Crystallinity analysis by the Rietveld-RIR method, J. Am. Ceram. Soc. 88 (2005) 3131–3136.
[15] D.U. Tulyaganov, Phase equilibrium in the fluroapatite–anorthite–diopside system, J. Am. Ceram. Soc. 83 (2000) 3141–3146.
[16] V.M.F. Marques, D.U. Tulyaganov, S. Agathopoulos, V.Kh. Gataullin, G.P. Kothiyal, J.M.F. Ferreira, Low temperature synthesis of anorthite based glass ceramics via sintering and crystallization of glass powder compacts, J. Eur. Ceram. Soc. 26 (2006) 2503–2510.
[17] C.S. Ray, Q. Yang, W. Huang, D.E. Day, Surface and internal crystallization in glasses as determined by differential thermal analysis, J. Am. Ceram. Soc. 79 (1996) 3155–3160.
[18] L. Barbieri, A.B. Corradi, I. Lancellotti, C. Leonelli, M. Montorsi, Experimental and computer simulation study of glasses belonging to diopside–anorthite system, J. Non-Cryst. Solids 345–346 (2004) 724–729.
[19] J.S. Petersen, G.E. Lofgren, Lamellar and patchy intergrowths in feldspars: experimental crystallization of eutectic silicates, Am. Miner. 71 (1986) 343–355.